Charge distribution and electric field effects on spatiotemporal patterns

A. F. Münster,[1] P. Hasal,[2] D. Šnita,[2] and M. Marek[2]
[1]*Institute of Physical Chemistry, University of Würzburg, Marcusstrasse 9-11, 97070 Würzburg, Germany*
[2]*Prague Institute of Chemical Technology, Department of Chemical Engineering, Technická 5, 166 28 Prague 6, Czech Republic*
(Received 18 February 1994)

Formation of spatial inhomogeneities in the electric field intensity and charge density arising due to an interaction of diffusion or migration with chemical reaction in an ionic version of the Brusselator are presented. The model involving spatial variations of electric field is compared to a conventional model assuming spatially homogeneous electric field. Predictions of the effects of electric field on spatial patterns differ. The existence of the field induced transitions between stationary and oscillatory states in a one-dimensional system and between striped and hexagonal patterns in a two-dimensional system is demonstrated.

PACS number(s): 41.20.−q

I. INTRODUCTION

The interaction of nonlinear chemical reactions with transport of components in reaction media plays a crucial role in formation of spatiotemporal and stationary patterns and has been proposed as a basis of morphogenesis (Turing [1], Meinhardt [2]). Electric field effects on propagation of chemical waves have been studied both experimentally and theoretically (Ortoleva *et al.* [3,4], Ševčíková *et al.* [5,6], Schütze, Steinbock, and Müller [7]) and effects on enzymatic reactions have been also discussed (Šnita and Marek [8]). Theoretical studies have been performed (Kondepudi and Prigogine [9], Almirantis and Kaufmann [10]) with the ionic Brusselator placed in one-dimensional (1D) reaction-diffusion medium with homogeneous electrical field. Local inhomogeneities in the electrical field intensity and electric charge density due to different mobilities of reacting ions were neglected. This approximation is valid for reaction media with the high ionic strength, high ionic mobilities, and slow chemical reactions. In other cases, the effects of electrical field inhomogeneities generated due to the mutual interaction of the electrically charged ions present in reaction-diffusion media must be incorporated into the mathematical model. Most chemical and biological reaction systems involve ionic compounds and experiments have shown that the fluxes of ionic components play an important role in signal propagation (Lechleiter and Clapham [11,12]) and in morphogenesis (Créton *et al.* [13]).

Here we use a mathematical model enabling us to compute local variations of the electric field intensity and charge density in the ionic reaction-diffusion systems where the effects of different ionic mobilities cannot be neglected.

II. THE MODEL

We used a modified Brusselator (cf. Nicolis and Prigogine [14] for the original scheme):

$$A \xrightarrow{k_1} X^+ + C^- , \tag{1}$$

$$B + X^+ \xrightarrow{k_2} Y^+ + D , \tag{2}$$

$$2X^+ + Y^+ \xrightarrow{k_3} 3X^+ , \tag{3}$$

$$X^+ \xrightarrow{k_4} X^{*+} , \tag{4}$$

$$X^{*+} + C^- \xrightarrow{k_5} E , \tag{5}$$

where X^{*+} is an unstable intermediate combining with C^- in the last reaction which is assumed to be very fast. The mass-balance equations for the components X^+, Y^+, and C^- are

$$\frac{\partial X}{\partial \tau} = -\nabla\cdot(-D_X\nabla X - D_X X\nabla\phi) + A - (B+1)X + X^2 Y , \tag{6}$$

$$\frac{\partial Y}{\partial \tau} = -\nabla\cdot(-D_Y\nabla Y - D_Y Y\nabla\phi) + BX - X^2 Y , \tag{7}$$

$$\frac{\partial C}{\partial \tau} = -\nabla\cdot(-D_C\nabla C + D_C C\nabla\phi) + A - X , \tag{8}$$

where $A = c_A/\sqrt{k_4^3/k_1^2 k_3}$, $B = c_B/(k_4/k_2)$, $C = c_C/\sqrt{k_4/k_3}$, $X = c_X/\sqrt{k_4/k_3}$, and $Y = c_Y/\sqrt{k_4/k_3}$ denote the dimensionless concentrations of respective components (A and B are supposed to be constants), c_i are molar concentrations. Dimensionless diffusion coefficients are $D_i = \mathcal{D}_i/(k_4 L^2)$, $[i \equiv C, X, Y]$, $\mathcal{D}_i$ are dimensional diffusivities, L is characteristic length of the system. Dimensionless electric potential is $\phi = \varphi/(RT/F)$, where φ is dimensional electric potential and F is Faraday constant. Dimensionless time is $\tau = k_4 t$. The fluxes of components X^+, Y^+, and C^- in Eqs. (6)–(8) are expressed by means of the Nernst-Planck relation (Newman [15]).

The electric field intensity (the electric potential gradient) $-\nabla\phi$ is commonly assumed to be constant with

respect to position. This assumption implies the electric conductivity to be constant throughout the system, therefore ionic mobility and ionic strength of the medium must be high. In other cases, however, we must consider variations of $-\nabla\phi$ along the spatial coordinate. To derive an explicit expression for $-\nabla\phi$ we have considered that the dimensionless electric charge density is

$$Q = X + Y - C \tag{9}$$

and the dimensionless electric current density is given by

$$I = J_X + J_Y - J_C \ , \tag{10}$$

where J_X, J_Y, and J_C are the dimensionless fluxes of respective components. The charge balance equation is

$$\frac{\partial Q}{\partial \tau} = -\nabla \cdot I \ . \tag{11}$$

When the local electroneutrality is assumed, then the electric current density is constant in a 1D system and

$$Q \simeq 0 \Longrightarrow C \simeq X + Y, \quad \nabla \cdot I \simeq 0 \ . \tag{12}$$

The electroneutrality condition (12) is a good approximation in macroscopic systems where typical dimension of a generated pattern is much larger than the Debye length of the reaction-diffusion medium. Then Eq. (12) can be used for evaluation of C with negligible inaccuracy. Typical dimensions of patterns observed in experiments ([5,6,16–18]) are within the range of hundreds of micrometers and are thus much larger than the Debye length (10^{-9} m). When inserting into Eq. (10) for component fluxes from the Nernst-Planck equation [cf. Eqs. (6)–(8)] and using $C = X + Y$ [cf. Eq. (12)] the electric field gradient $-\nabla\phi$ can be expressed as

$$-\nabla\phi = \frac{I + (D_X - D_C)\nabla X + (D_Y - D_C)\nabla Y}{(D_X + D_C)X + (D_Y + D_C)Y} \ . \tag{13}$$

The charge density Q is related to the electric field intensity and/or electric potential according to the Gauss law of electrostatics (Newman [15])

$$\nabla^2\phi = \nabla E = -\frac{L}{l_D} Q \ , \quad E \equiv -\nabla\phi \ , \tag{14}$$

where L is typical (macroscopic) dimension of the system and l_D is the Debye length. The fraction $-L/l_D$ takes very large values. Therefore, the spatial gradient of E is of significant magnitude despite the negligible value of Q [cf. Eq. (12)]. This fact is a contradiction to the commonly adopted assumption of spatially homogeneous electric field.

In the following text, we will call the model based on the assumption of homogeneous electric field (constant E) as the constant electric field model (CEFM) and the model using Eq. (13) for evaluation of local electric field intensity as the variable electric field model (VEFM).

III. RESULTS AND DISCUSSION

The ionic character of the intermediates X^+ and Y^+ leads to a decrease in the amplitude and wave number of the pattern if compared to the conventional nonionic Brusselator [cf. Fig. 1(a)]. Local inhomogeneities in the electric field intensity arise even in the absence of an externally applied electric field (or current) reflecting different mobilities of the ionic components [cf. Fig. 1(b)]. Weak electric current shifts the profile of the electrical field intensity to lower mean value. Figure 1(b) displays also a fine structure of the charge density distribution in the absence of an external electric field.

The externally applied electric field causes not only spatial distortion of the steady pattern developed in its absence, but also a formation of coexistent regions with qualitatively different spatiotemporal patterns within the system (cf. Fig. 2): The temporal oscillations arise with an amplitude varying markedly along the system axis. The amplitude (concentration of X) at the left boundary

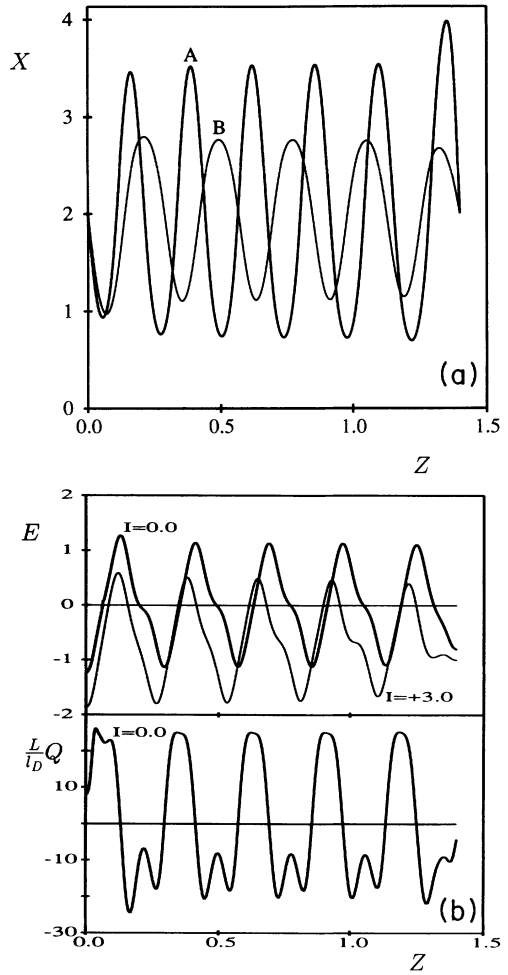

FIG. 1. (a) Asymmetric profiles of X for the conventional (line A) and ionic (line B) Brusselator without an externally applied electrical current; (b) local electrical field intensity and charge density profiles for the ionic Brusselator (VEFM model). The charge density was computed according to Eq. (14) and is scaled by the ratio of a characteristic length of the system and the Debye length. Parameters are $L = 1.4$, $A = 2.0$, $B = 5.2$, $D_X = 1.6 \times 10^{-3}$, $D_Y = 6.0 \times 10^{-3}$, and $D_C = 1.0$. Boundary conditions are $X_0 = X_L = 2.0$ and $Y_0 = Y_L = 2.6$.

(dimensionless spatial coordinate $Z=0$) is of the order $10^{-3}-10^{-2}$. The amplitude of temporal oscillations is several times higher at the right boundary ($Z=1.4$) due to the suppressed buffering capacity of the counterion C^- at the vicinity of the cathode. The width of the low amplitude oscillatory region increases with the increasing value of the current passing through the system [cf. Figs. 2(a), 2(b)]. The wavelike pattern is generated near the right boundary and moves to the left where it is annihilated by an interaction with the stable pattern. The amplitude of the waves is modulated by the amplitude of temporal oscillations. The frequency of temporal oscillations increases sharply with the current intensity [cf. Figs. 2(a), 2(b)]. The spatiotemporal pattern of the electric field intensity [see Fig. 2(c)] exhibits similar behavior as the X pattern in Fig. 2(b). The value of E reaches its maximum at the left boundary due to low ionic strength and, therefore, low electric conductivity of the medium [cf. Fig. 3(a)].

The CEFM model yields only the steady pattern (not shown in the figure) at the value of electric field intensity $E=10.67$ [the time and spatial average of $E(z,t)$ in Fig.

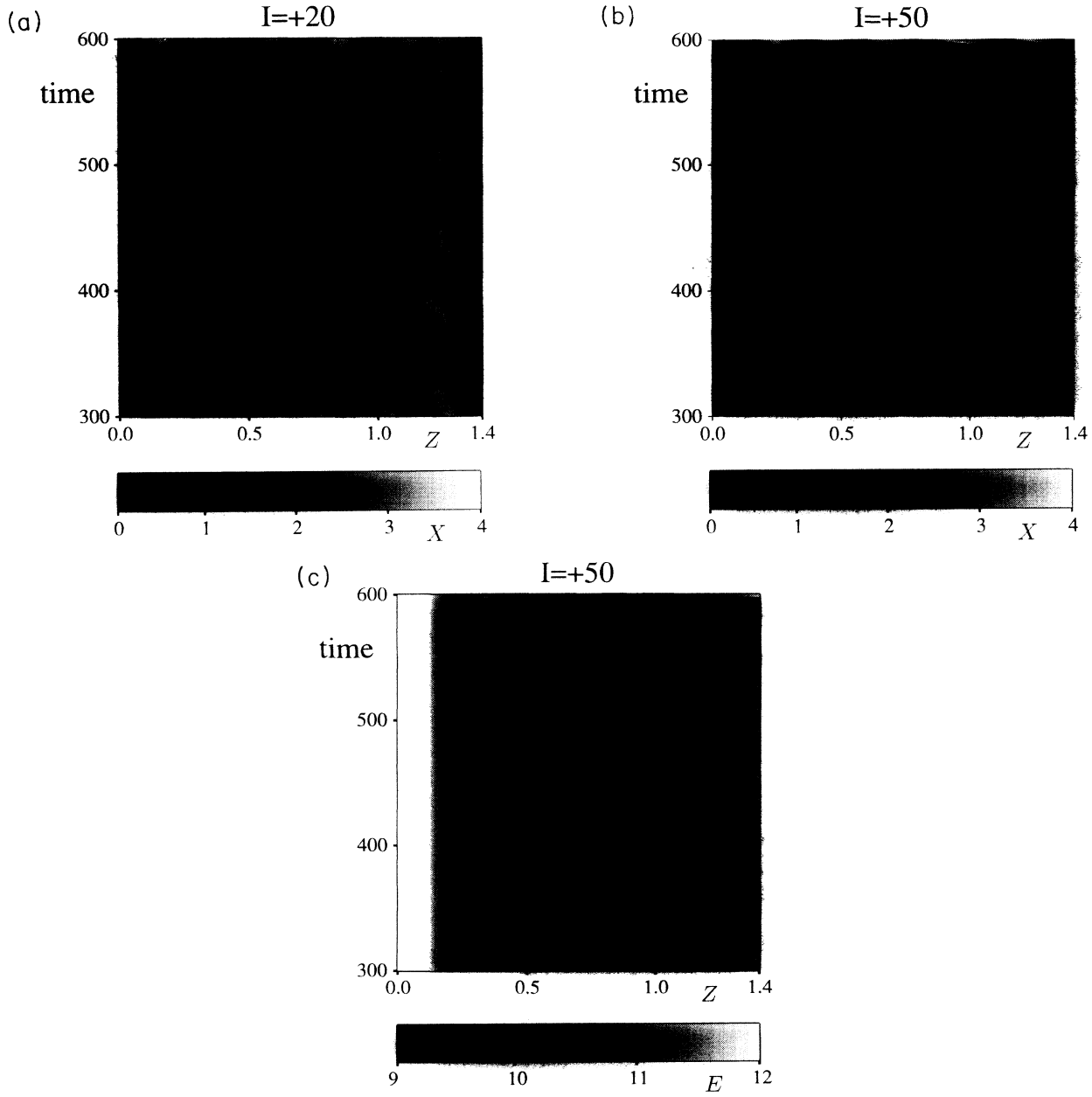

FIG. 2. Density plots of spatiotemporal patterns of X and E for the ionic Brusselator (VEFM model). (a) Plot of X at $I=+20.0$. (b) Plot of X at $I=+50.0$. (c) Plot at E at $I=+50.0$. Parameters are $L=1.4$, $A=2.0$, $B=5.9$, $D_X=1.6\times10^{-3}$, $D_Y=6.0\times10^{-3}$, $D_C=1.0$. Initial conditions are the steady pattern developed under zero external current. Boundary conditions are zero diffusional fluxes.

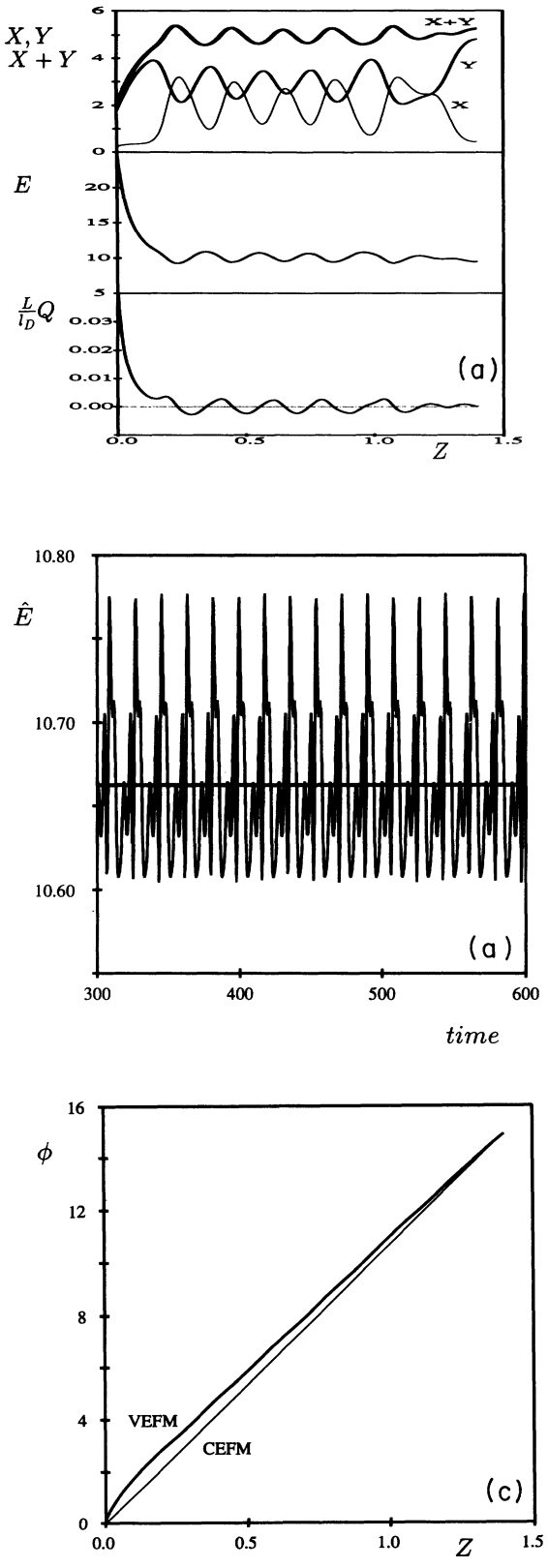

FIG. 3. (a) Snapshots of spatial profiles at time $t=300$ (VEFM model). (b) Temporal oscillations of spatially averaged electric field intensity (average temporal value $\bar{E}=10.67$). (c) Electric potential profiles for VEFM and CEFM models (for parameters see Fig. 2).

2(a)]. This stable pattern is only slightly distorted by the applied electric field if compared to the steady state pattern generated in the absence of the external field. The onset of oscillations (traveling waves) in the CEFM model is shifted towards much higher intensities of applied electric field if compared to the average field intensity in the VEFM model.

The snapshots of profiles generated by the VEFM model at $I=+50$ in Fig. 3(a) are shown to illustrate the intrinsic structure of the system. The low concentration of X^+ ions at the left boundary (anode) results in high electric field intensity and charge density within this region. The concentration profiles in other parts of the system have wavy character, therefore their gradients change the sign along the system. The spatially averaged value of $\hat{E}$ for the VEFM model is depicted in Fig. 3(b) and we can observe low-amplitude high-frequency oscillations. The temporal oscillations of the spatially averaged charge density and the electric potential at the right boundary follow the oscillations of $\hat{E}$. Despite their low amplitude these oscillations play a crucial role in forming the global oscillatory behavior of the system. The electric potential profiles in Fig. 3(c) (spatial integrals of E) show relatively little difference between the results of the VEFM and CEFM models. The significance of the local gradients of E and Q for the pattern formation is emphasized.

Patterns evolving in a 2D system with the CEFM model are shown in Fig. 4. Here the homogeneous electrical field is assumed directed parallel to the spatial coordinate Z_1. Transitions between striped and hexagonal Turing patterns occur under increasing electrical field intensity

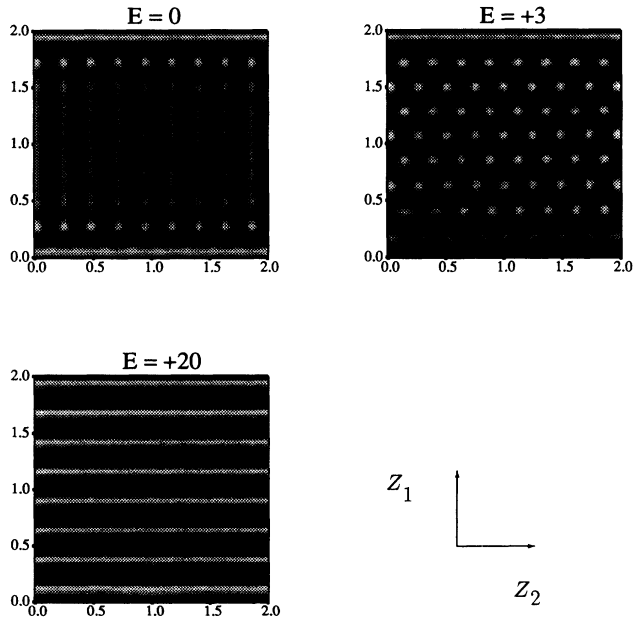

FIG. 4. 2D steady state pattern of X on a square (side length $L=2.0$) for the ionic Brusselator (CEFM model with electric field parallel to Z_1 and zero field gradient parallel to Z_2). Boundary conditions are $X_{Z_1=0}=X_{Z_1=2}=2.0$ and $Y_{Z_1=0}=Y_{Z_1=2}=2.6$, the zero diffusion flux boundaries at $Z_2=0$, and $Z_2=2.0$ (for parameters see Fig. 1).

in a manner similar to transitions described in the CIMA reaction experiments [(16,17]).

In conclusion, formation of spatiotemporal and stationary spatial structures in ionic reaction-diffusion systems leads to inhomogeneities of the local electrical field intensity and charge density distribution inside the system. Externally applied electrical fields can induce oscillatory behavior in part of the system suppressing the formation of the stationary patterns. The predictions of the onset of wavelike regimes differ for both models. In a spatially two-dimensional system an external electrical field can switch between different types of Turing patterns thereby controlling the pattern generating process.

ACKNOWLEDGMENTS

This work was supported by Czech Grant Agency, Grant No. 104/93/0272. A. F. Münster thanks Professor M. Marek and his group for hospitality during his stay at Department of Chemical Engineering of Prague Institute of Chemical Technology.

[1] A. Turing, Philos. Trans. R. Soc. London, Ser. B **237**, 37 (1952).
[2] H. Meinhardt, *Models of Biological Pattern Formation* (Academic, London, 1982).
[3] P. Ortoleva, Physica D **26**, 67 (1987).
[4] S. Schmidt and P. Ortoleva, J. Chem. Phys. **74**, 4488 (1981).
[5] H. Ševčíková and M. Marek, Physica D **9**, 140 (1983).
[6] H. Ševčíková. M. Marek, and S. C. Müller, Science **257**, 951 (1992).
[7] J. Schütze, O. Steinbock, and S. C. Müller, Nature **356**, 45 (1992).
[8] D. Šnita and M. Marek, *Interaction of Electromagnetic Field with Enzymatic Reactions and pH Effects,* edited by S. Aiba (University of Tokyo Press, Tokyo, 1987), pp. 337–365.
[9] D. K. Kondepudi and I. Prigogine, Physica A **107**, 1 (1981).
[10] Y. Almirantis and M. Kaufmann, Int. J. Bif. Chaos **2**, 51 (1992).
[11] J. D. Lechleiter and D. E. Clapham, Nature **350**, 505 (1991).
[12] J. D. Lechleiter and D. E. Clapham, Cell **69**, 283 (1992).
[13] R. Créton, D. Zivkovic, J. E. Speksnijder, and M. R. Dohmen, Roux's Arch. Dev. Biol. **201**, 346 (1992).
[14] G. Nicolis and I. Prigogine, *Self-Organization in Non-equilibrium Systems* (Wiley, New York, 1977).
[15] J. S. Newman, *Electrochemical Systems* (Prentice Hall, New Jersey, 1973), Chap. 12.
[16] Q. Ouyang and H. L. Swinney, Nature **352**, 610 (1991).
[17] I. Lengyel, S. Kádár, and I. R. Epstein, Science **259**, 493 (1993).
[18] H. Meinhardt, Rep. Prog. Phys. **55**, 797 (1992).

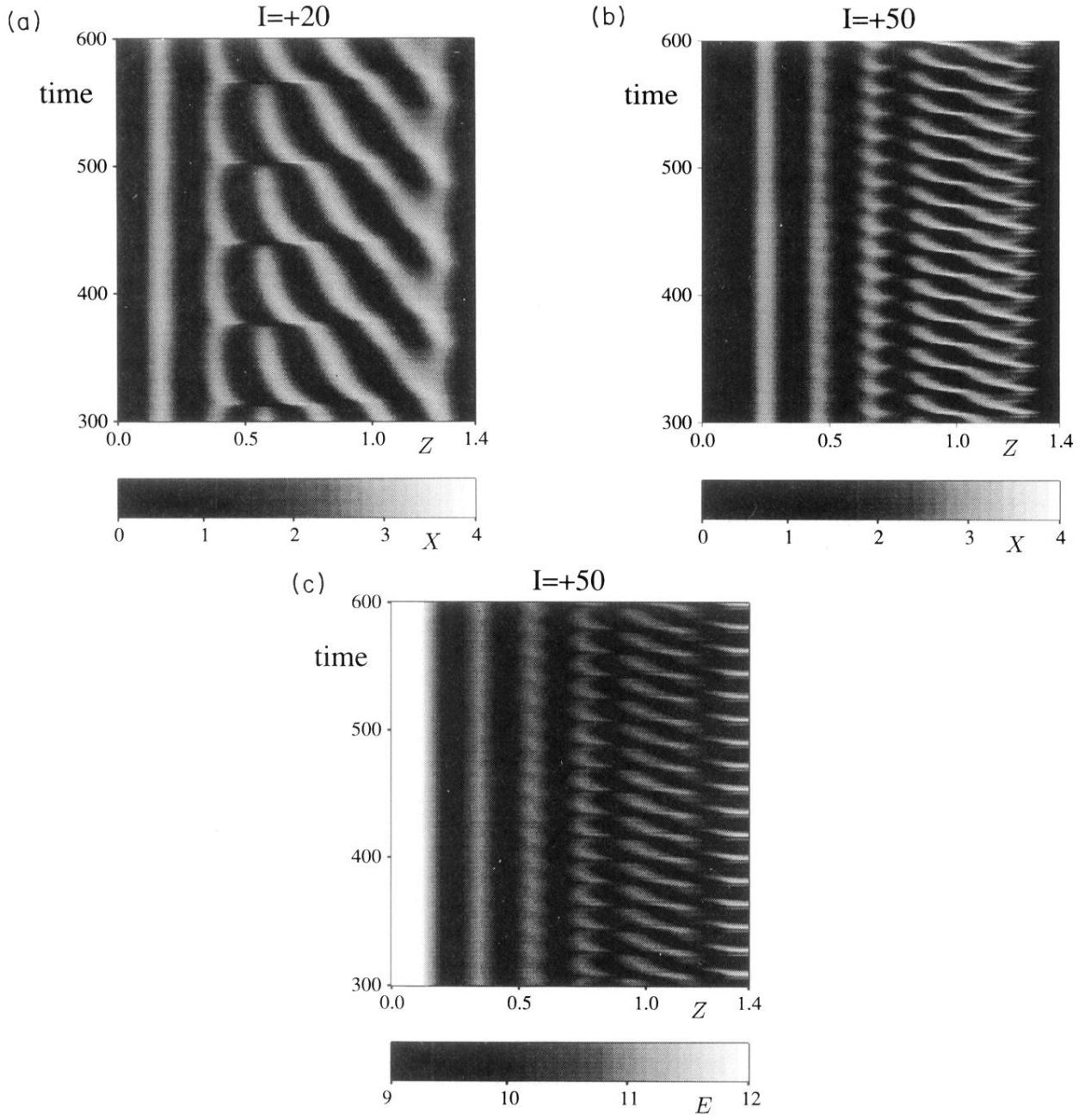

FIG. 2. Density plots of spatiotemporal patterns of X and E for the ionic Brusselator (VEFM model). (a) Plot of X at $I=+20.0$. (b) Plot of X at $I=+50.0$. (c) Plot at E at $I=+50.0$. Parameters are $L=1.4$, $A=2.0$, $B=5.9$, $D_X=1.6\times10^{-3}$, $D_Y=6.0\times10^{-3}$, $D_C=1.0$. Initial conditions are the steady pattern developed under zero external current. Boundary conditions are zero diffusional fluxes.

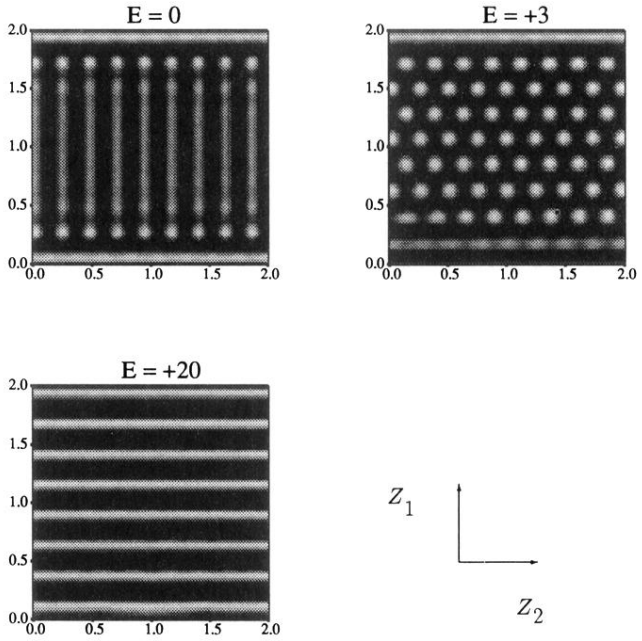

FIG. 4. 2D steady state pattern of X on a square (side length $L=2.0$) for the ionic Brusselator (CEFM model with electric field parallel to Z_1 and zero field gradient parallel to Z_2). Boundary conditions are $X_{Z_1=0}=X_{Z_1=2}=2.0$ and $Y_{Z_1=0}=Y_{Z_1=2}=2.6$, the zero diffusion flux boundaries at $Z_2=0$, and $Z_2=2.0$ (for parameters see Fig. 1).